Defence Technology xxx (xxxx) xxx

Contents lists available at ScienceDirect

Defence Technology

journal homepage: www.keaipublishing.com/en/journals/defence-technology

The deformation and failure mechanism of cylindrical shell and square plate with pre-formed holes under blast loading

Wei Li [a], Peng Wang [a], Gao-peng Feng [a], Yong-gang Lu [a], Jun-zheng Yue [b], Hui-min Li [a, *]

[a] Institute of System Engineering, CAEP, Mianyang 621900, Sichuan, China
[b] Institute of Mechanics, Chinese Academy of Science, Beijing 100190, China

ARTICLE INFO

Article history:
Received 10 April 2020
Received in revised form
6 June 2020
Accepted 16 June 2020
Available online xxx

Keywords:
Pre-formed holes
Cylindrical shell and square plate
Deformation mechanism
Failure mechanism

ABSTRACT

The deformation and failure mechanism of cylindrical shells and square plate with pre-formed holes under blast loading were investigated numerically by employing the Ansys 17.0 and Ls-Dyna 971. To calibrate the numerical model, the experiments of square plates with pre-formed circle holes were modeled and the numerical results have a good agreement with the experiment data. The calibrated numerical model was used to study the deformation and failure mechanism of cylindrical shells with pre-formed circle holes subjected to blast loading. The structure response and stress field changing process has been divided into four specific stages and the deformation mechanism has been discussed systematically. The local and global deformation curves, degree of damage, change of stress status and failure modes of cylindrical shell and square plate with pre-formed circular holes are obtained, compared and analyzed, it can be concluded as: (1) The transition of tensile stress fields is due to the geometrical characteristic of pre-formed holes and cylindrical shell with arch configuration; (2) The existence of pre-formed holes not only lead to the increasing of stress concentration around the holes, but also release the stress concentration during whole response process; (3) There are three and two kinds of failure modes for square plate and cylindrical shell with pre-formed holes, respectively. and the standoff distance has a key influence on the forming location of the crack initiating point and the locus of crack propagation; (4) The square plate with pre-formed holes has a better performance than cylindrical shell on blast-resistant capability at a smaller standoff distance, while the influence of pre-formed holes on the reduction of blast-resistant capability of square plate is bigger than that of cylindrical shell.

1. Introduction

For the conventional warhead or the metal container storing flammable explosive gas, fragments and blast loading will be incurred under initiation or accident stimuli. Under the combined action of these two kinds of loading, what the shell structures such as vehicles, airplanes, buildings, cabins of ship and a large number of potentially containers subjected to is not the accumulation of effects of fragments and blast loading separately, but the damage effect of blast loading applied on the perforated structures or on the contrary. According to Forsén et al. [1], the mechanism and the degree of damage of the coupled effect will be more complicated and serious, respectively.

The coupled effect of some structures under the combined action of fragments and blast loading has been studied by experiments and numerical simulations. He et al. [2] carried out a blast experiment to study the coupled effect of protective door under the combined loading of fragments and blast wave. Nystrom et al. [3] investigated the combined action of blast and fragment loading on the reinforced concrete wall through numerical simulation method. The damage effect of the wall subjected to blast loading, fragment loading, and combined blast and fragment loading were compared, which indicates that the coupled effect has a larger damage than others. Zhang et al. [4] investigated the deformation failure modes and damage mechanisms of steel-GFRP-steel sandwich plates under blast waves with high-velocity fragments and found that the damage degree under the combined action of these two loadings is much higher than that under blast waves only. Liu et al. [5] compared the damage effect and obtained the damage modes of

* Corresponding author.
E-mail address: 414liw@caep.cn (H.-m. Li).
Peer review under responsibility of China Ordnance Society

https://doi.org/10.1016/j.dt.2020.06.014

helicopter rotor under the combined action of fragments and blast loading with that under the action alone of them by numerical simulation. Hou et al. [6] conducted experiments adopting cast TNT and prefabricated fragments to study the damage characteristics, failure modes and the protective mechanism of sandwich bulkhead under the impact of shock and high-velocity fragments and pointed out that the main failure mode of the front plate is the combination of large deformation and large amounts of perforation holes while that of the back plate is only large deformation.

Because of the complexity on the response process and mechanism of the combined action, it is difficult to control the influent factors in experiment. Considering the fragments arriving the structures earlier than blast loading at relatively farther distance [7,8] in according to the attenuation rules of blast wave and fragments velocity in air, the approach of structures with pre-formed holes subjected to blast loading is widely adopted to decouple the complex coupled effect. Considering plastic hinge formation and extensional effects, Schleyer et al. [9] applied an energy approach to solve the large deformation problem of square plates with either square or circular holes under transverse pulse pressure loading and conducted experiments to validate this approach. Assuming that the fragments perforate the square plates before the pressure load arrives, Rakvåg et al. [10] carried out experiments that plates with pre-formed holes are subjected to controlled pressure pulses and analyzed deformation modes. In addition, the difference of deformation around the pre-formed holes between standard Lagrangian and Fully coupled FSI simulations was discussed. Hou et al. [11,12] studies the deformation rules with change of the number and diameter of holes and proposed a formula to calculate the midpoint deformation of plate with holes. Carrying out experiments and adopting numerical simulation for the response of square plates with pre-formed holes under blast loading, Li et al. [13] investigated the difference of deformation, failure and damage in three kinds of hole shapes, quantitatively. Wu et al. [14] conducted experiments and numerical simulation to investigate the stress concentration, deformation, energy changes and failure of a metal cylindrical pipeline with pre-formed holes under blast loading, in addition, the capability to resist blast loading with change of hole-spacing and stand-off distance were analyzed. Aune et al. [15] et al. studies the dynamic response of the steel plates with and without pre-formed holes under the blast loading generated by a shock tube facility, the deformation is quantified and measured by 3D-DIC,which is used to compare the failure with numerical simulation results, in addition, the crack propagation was observed by using adaptive mesh refinement and element erosion.

In order to obtain the deformation and failure mechanism of cylindrical shells and square plates with pre-formed holes, the present research is concerned with the distribution and quantitation of stress concentration, local and global deformation, degree of damage, change of stress status and failure modes generated on cylindrical shells and square plates with pre-formed holes under blast loading, which not only represents an extension of the previous works on the perforated structures but also describes the deformation and failure mechanism from multi-viewpoints. The commercial software Ls-Dyna 971 was applied to investigate the dynamic responses and deformation of cylindrical shells and square plates with pre-formed holes under blast loading. To calibrate the accuracy of the numerical model, the numerical results of a series of square plates with pre-formed circular holes were compared with the experimental results recorded by Li et al. [13]. The calibrated models were then employed to perform the simulations of the cylindrical shells with pre-formed circular holes. The comparison of structure response process, stress nephogram, local and global deformation, degree of damage, change of stress status and failure modes between cylindrical shell and square plate with pre-formed circular holes under blast loading have been discussed in this study. In addition, the stages of stress concentration are classified and the deformation and failure mechanism are analyzed. Details are presented in the following sections.

2. Numerical model calibrations

The commercial software Ansys 17.0 and Ls-Dyna 971 was used to establish the numerical model and perform numerical analysis [16]. A non-linear, explicit finite element numerical method of Ls-Dyna 971 was adopted to model the large inelastic deformation and failure. Reliable and accurate numerical predictions of structural response to blast load have been approved [17–20]. So the numerical simulation of the structural responses of the cylindrical shells with pre-formed holes under blast loading was carried out by this software.

To validate the accuracy and reliability of the numerical model in this paper, a square plate with pre-formed circular holes tested by Li et al. [13] was used to calibrate the model. A total of nine explosion tests were conducted in the experiments, three of them were related to circular holes under different charges of 550 g, 650 g and 750 g, respectively. The same structural parameters were adopted in these three tests including a square plate with the length of 1000 mm and the thicknesses of 4 mm, the core loading area of 600 mm × 600 mm, nine holes with the diameter of 80 mm, the distance of 150 mm between centers of two adjacent holes and the distance between charge and the square plate is 250 mm(defined as standoff distance in the following), as shown in Fig. 1. There are 76 bolts with diameter of 20 mm used to fix the square plates with pre-formed circular holes between the supporting frame and the cover plate. The supporting frame and the cover plate have the same breadth and thickness of 100 mm and 30 mm, respectively. The maximum midpoint displacement, the middle and 1/4 locus deformation curves of square plates were measured by laser scanning reverse forming technique and the reverse post-engineering software Geomagic Qualify. Selected test data were used to calibrate the numerical model established in this study.

2.1. Element, mesh, boundary conditions and contact modeling

Since the square plate with circular holes, the supporting frame and the cover plate are all symmetric about two middle planes which are perpendicular to each other, a quarter of the plates and frames were modeled, as shown in Fig. 2. The numerical models have been established by the commercial software Ansys 17.0. After carrying out a mesh convergence analysis, a feature element size of 5 mm was selected to be optimal for the shell and solid elements, which balanced the numerical element sensitivity requirement, the

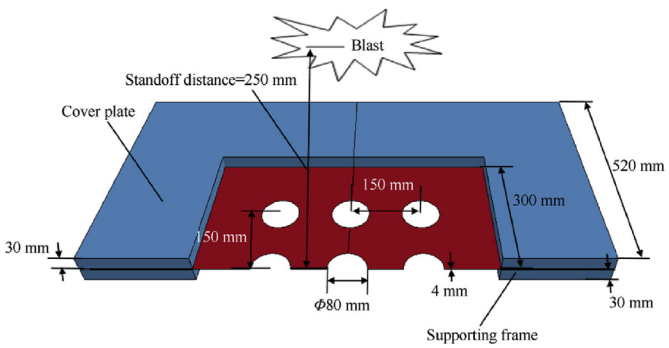

Fig. 1. The schematic diagram of the experiment settings.

Please cite this article as: Li W et al., The deformation and failure mechanism of cylindrical shell and square plate with pre-formed holes under blast loading, Defence Technology, https://doi.org/10.1016/j.dt.2020.06.014

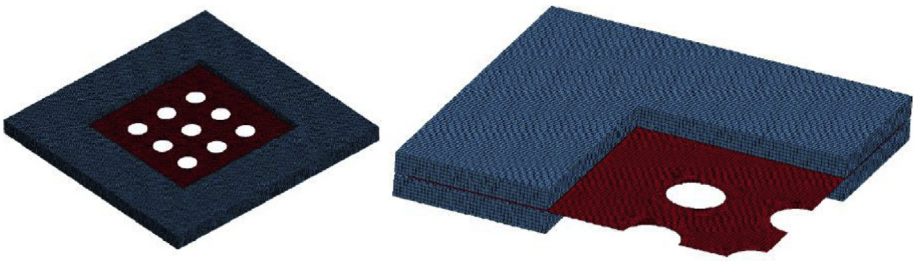

(a) Whole model (b) 1/4 model

Fig. 2. Finite element model of square plate with pre-formed holes.

accuracy of the results and the computational efficiency. The square plate with pre-formed circular holes was modeled by Belyschko-Tasy four -node shell elements [21], the supporting frame and the cover plate were modeled by eight-node solid elements.

To simulating the action of bolts used in the experiments to fix the square plate, two approaches of boundary conditions were considered in this numerical simulation. The first approach (BC.1) is more close to represent the experimental conditions, so the nodal constraints were used at positions of bolts in the square plate, the supporting frame and the cover plate, as showed in Fig. 3. The second approach (BC.2) is a simplification of the first approach. The nodal constraints were only used at positions of bolts in the square plate, as showed in Fig. 4.

The *CONTACT_AUTOMATIC_SINGLE_SURFACE model embed in Ls-Dyna 971 was adopted to prevent the penetration between the square plate, the supporting frame and the cover plate, which is a single surface contact defined wholly by the slave side with a contact static and a contact dynamic friction value of 0.28 and 0.20, respectively. In addition, shell thickness is also considered in this contact model, which is suitable to simulate the structures comprised by shells.

2.2. Material model

According to the experiments of Li et al. [13], Q345 steel was adopted as material of square plates. With quite well describing of the hardening effect, strain rate effect and temperature softening effect of metallic materials [22], the Johnson-Cook strength model of Ls-Dyna 971 named *MAT_JOHNSON_COOK was used to represent the mechanical behavior of Q345 and to model the dynamic response of square plate with pre-formed circular holes under blast loading. The model is expressed as Eq. (1):

$$\sigma_E = (A + B(\varepsilon_E)^n)\left(1 + C\ln\frac{\dot{\varepsilon}}{\dot{\varepsilon}_0}\right)\left[1 - \left(\frac{T - T_r}{T_m - T_r}\right)^m\right] \quad (1)$$

where A, B, C, n and m are the constants of the material and given in Table 1, σ_E is the equivalent stress, $\varepsilon_E$is the effective plastic strain, $\dot{\varepsilon}$is the strain rate, $\dot{\varepsilon}_0$is the reference strain rate in quasi-static experiment, T is the current temperament, T_r is the room temperature and the T_m is the melting temperature of the material.

The damage model embed in Johnson-Cook model is based on the concept of cumulative damage generated by plastic strain.

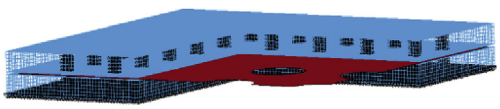

Fig. 3. Boundary condition 1 (B.C.1).

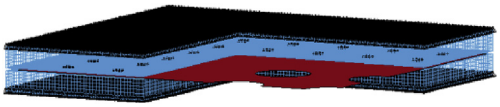

Fig. 4. Boundary condition 2 (B.C.2).

Damage factor D is defined as Eq. (2):

$$D = \sum \frac{\Delta\varepsilon}{\varepsilon_f} \quad (2)$$

where $\Delta\varepsilon$is the increment of effective plastic strain for every integration cycle. ε_f is the effective fracture strain when the fracture occurs, at the moment, the damage factor D is 1. The effective fracture strain ε_f is expressed as Eq. (3):

$$\varepsilon_f = [D_1 + D_2\exp(-D_3\eta)]\left[1 + D_4\ln\left(\frac{\dot{\varepsilon}}{\dot{\varepsilon}_0}\right)\right]\left[1 + D_5\frac{T - T_r}{T_m - T_r}\right] \quad (3)$$

where D_1, D_2, D_3, D_4 and D_5 are the damage constants of the material and are given in Table 1, η is the stress triaxiality factor.

The keyword *EOS_GRUNEISEN was adopted as the equation of state of Q345 steel and the pressure for compressed materials as Eq. (4) [16],:

$$p = \frac{\rho_0 C^2\mu\left[1 + \left(1 - \frac{\gamma_0}{2}\right)\mu - \frac{a}{2}\mu^2\right]}{\left[1 - (S_1 - 1)\mu - S_2\frac{\mu^2}{\mu+1} - S_3\frac{\mu^3}{(\mu+1)^2}\right]} + (\gamma_0 + a\mu)E \quad (4)$$

where C is the intercept of the v_s-v_p curve; S_1, S_2 and S_3 are the coefficients of the slope of the v_s-v_p curve; γ_0 is the Gruneisen gamma; a is the first order volume correction to γ_0; and $\mu = \rho/\rho_0$-1.

The Johnson-cook parameters of Q345 steel listed in Table 1 were obtained by Li [13] who adopt MTS universal material testing machine and Split Hopkinson Tension Bar (SHPB) to carrying out quasi-static tension test and dynamic tensile test for measuring the static and dynamic tensile mechanical properties of Q345, respectively. These parameters have been used to simulate the numerical models established by Li [13], and the maximum midpoint displacement of numerical simulation has a good agreement with the experimental results. In addition, the maximum midpoint displacement and the local deformation around the holes are obtained by numerical simulation carried out by this paper and agree well with the experimental results reported by Li [13], which has described in section 2.4. As a result, the Johnson-cook parameters of Q345 steel listed in Table 1 has been demonstrated that the material parameters used in the simulations truly represent the actual physical properties of the material investigated.

Please cite this article as: Li W et al., The deformation and failure mechanism of cylindrical shell and square plate with pre-formed holes under blast loading, Defence Technology, https://doi.org/10.1016/j.dt.2020.06.014

Table 1
Johnson-cook parameters of Q345 steel [13].

A/MPa	B/MPa	n	C	m	T_m/K	D_1	D_2	D_3	D_4	D_5
356	760	0.62	0.056	0.94	1798	0.296	1.184	−1.465	0.005	8.07

2.3. Blast load modeling

In this study, blast loading was generated by the CONWEP(Conventional Weapons Effects Program) empirical model implemented as the *LOAD_BLAST [16] in Ls-Dyna 971. The CONWEP algorithms developed by Kingery and Bulmash [23] accounts for angle of incidence by combining the reflected pressure(normal-incidence) value and the incident pressure (side-on-incidence) value, which is a quite accurate method to load air-blast free-field blast wave. The pressure can be calculated by Eq. (5):

$$P_{\text{load}} = P_{\text{reflected}} \cdot \cos^2\theta + P_{\text{incident}} \cdot \left(1 + \cos^2\theta - 2\cos\theta\right) \tag{5}$$

where θ is the angle of incidence; P_{incident} is the incident pressure; $P_{\text{reflected}}$ is the reflected pressure.

The keyword *LOAD_BLAST can provide the blast pressure on the certain surfaces predefined by the keyword *LOAD_SEGMENT_SET. The parameters required for *LOAD_BLAST include equivalent mass of TNT explosive, the spatial coordinates of the detonation point, the initiative time and the type of blast. According to the experiments of Li et al. [13], the mass of charge are 550 g, 650 g and 750 g and are all with the standoff distance of 250 mm.

3. Result and discussions

Fig. 5 compares the displacement time history of center point of square plate with pre-formed holes between two kinds of boundary conditions for 550g charge with the standoff distance 250 mm. The results indicate that there is almost no difference of displacement time history curves between B.C.1 and B.C.2, while the computational efficiency of B.C.2 is higher than that of B.C.1. Therefore, the B.C.2 was employed in the subsequent models. In addition, due to the clamped frame boundary, the weakening of shock wave and the increasing deformation energy of square plate, the displacement of center point begins to rebound and a definitely decreasing occurs at 2 ms.

In order to validate the agreement between the numerical results and experimental data reported [13] of the square plate with pre-formed circular holes under blast loading, the permanent displacements of max-deformation point(center point) are compared for three cases with different weight charge (550 g, 650 g and 750 g) with the standoff distance 250 mm. As shown in Fig. 6, the numerical results of permanent displacement of max-deformation point agree well with the experimental data of that and the maximum errors were all less than 5%.

Because of the local deformation occurring around the circular holes, it is not enough to validate the numerical models by comparing the permanent displacement of max-deformation point between the numerical results and experimental data. In this study, the comparison is further performed by considering the deformation curves of the plate center locus and 1/4 locus which is shown as red solid line in Fig. 7. The deformation curves of the center locus and 1/4 locus of the square plate with pre-formed holes under blast loading of 750 g TNT charge with the standoff distance 250 mm are illustrated in Fig. 8.

The numerical results and experimental data of deformation curves of the center locus are compared as shown in Fig. 8(a). There are three gaps on the deformation curves, which represent the projections of the pre-formed circular holes on the center locus. The local deformation occurring around the circular holes and on the rest of square plate both have a good agreement between the numerical results and experimental data. The numerical results of deformation curves of the 1/4 locus also agree well with the experimental data, as shown in Fig. 8(b).

The comparison above indicates that the numerical model established in this study gives reliable predictions of square plate with pre-formed circular holes under blast loads and can be applied in subsequent calculation and analysis.

4. Numerical simulation

The calibrated numerical model above was adopted to carry out the simulation of dynamic response, deformation and damage of cylindrical shell with pre-formed circular holes under external blast loading. The response and damage quantities such as the permanent displacement and the displacement of the center locus and 1/4 locus, the degree of damage, the dynamic stress concentration factor and the change of stress status around the pre-formed circular holes and failure modes were analyzed and compared with that of the square plate with pre-formed circular holes to examine the capacities of blast-resistance.

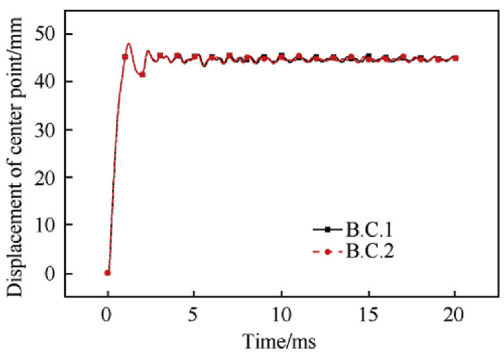

Fig. 5. Comparison of displacement time history of center point between two kinds of boundary conditions.

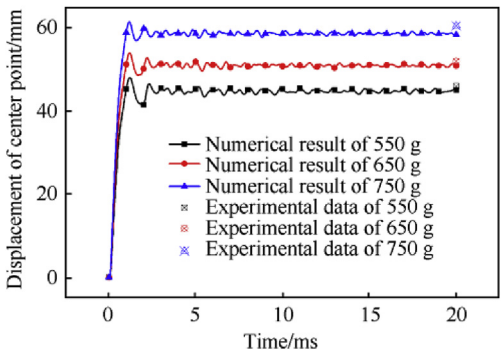

Fig. 6. Comparison of permanent displacement of max-deformation point between the experimental data and the numerical results.

Please cite this article as: Li W et al., The deformation and failure mechanism of cylindrical shell and square plate with pre-formed holes under blast loading, Defence Technology, https://doi.org/10.1016/j.dt.2020.06.014

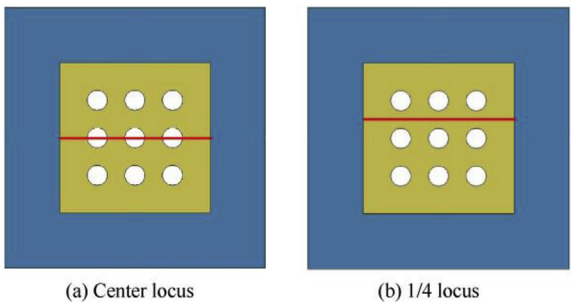

Fig. 7. The schematic diagram of center locus and 1/4 locus.

4.1. The configurations of cylindrical shell with pre-formed circular holes

In order to compare the capacities of blast-resistance between cylindrical shell and square plate with pre-formed circular holes, keeping the same size of holes, the number of holes, the hole-spacing, the loading area and the thickness of shell/plate, the equivalent cylindrical shell with pre-formed circular holes were considered in this study. The schematic diagram of equivalent structure were shown in Fig. 9.

4.2. Modeling

The 750 g TNT charge was ignited with the standoff distance 250 mm above the cylindrical shell as shown in Fig. 9. Blast load was modeled by adopting the CONWEP empirical model implemented in Ls-Dyna. The cylindrical shell with pre-formed circular holes was modeled with Belyschko-Tasy four -node shell elements of 5 mm size, the supporting frame and the cover plate were modeled by eight-node solid elements of 5 mm size. The material properties, type of elements, mesh method, blast load modeling, boundary conditions and contact modeling are same as the calibration simulation, as shown in Fig. 10.

5. Simulation results and discussion

The simulation results presented and discussed about the comparison between cylindrical shell and square plate with pre-formed circular holes in six sections include: the structure response process and the deformation mechanism; the

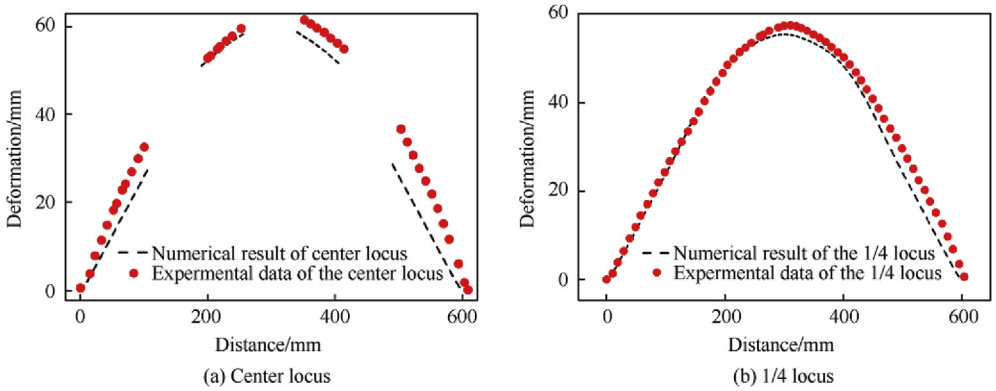

Fig. 8. Comparison of permanent deflection at the center locus and 1/4 locus between the experimental data and the numerical results.

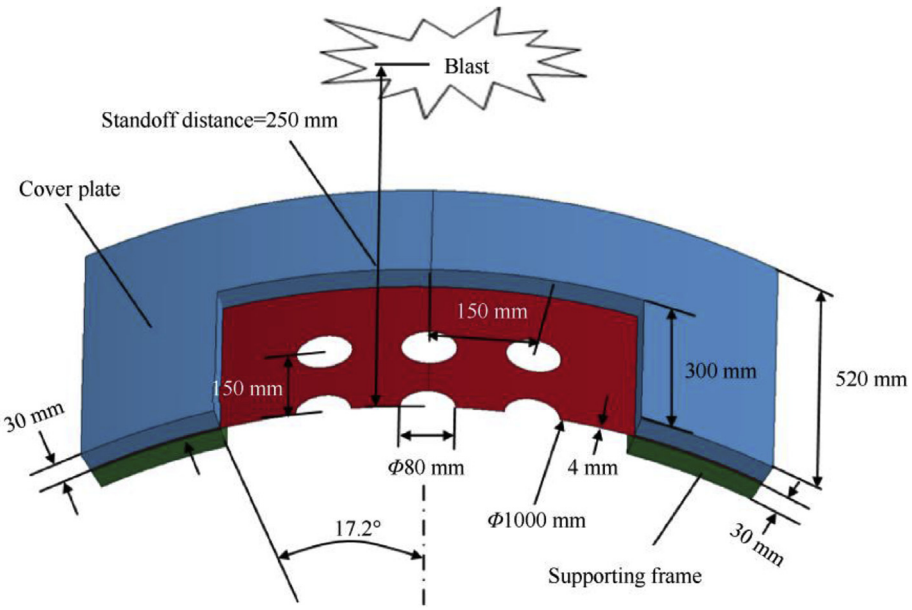

Fig. 9. The schematic diagram of cylindrical shell with pre-formed holes.

Please cite this article as: Li W et al., The deformation and failure mechanism of cylindrical shell and square plate with pre-formed holes under blast loading, Defence Technology, https://doi.org/10.1016/j.dt.2020.06.014

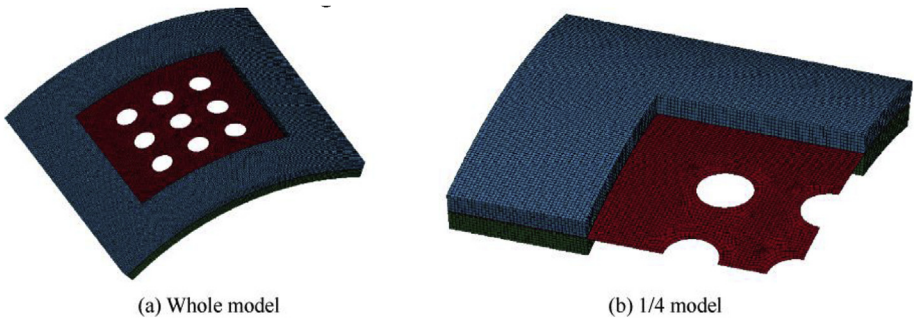

Fig. 10. Finite element model of cylindrical shell with pre-formed holes.

deformation curves, degree of damage, dynamic stress concentration factor, change of stress status and failure modes. These were individually described in Section 4.1-4.6.

5.1. The structure response process and the deformation mechanism

Fig. 11 show the structure response process and stress field of square plate and cylindrical shell with pre-formed circular holes under blast loading. The operating condition of them in the simulation were 750 g TNT charge and 250 mm standoff distance. According to the characteristic of the structural response of cylindrical shell with pre-formed circular holes, the process is divided into four specific stages, that is, First stage-In control of axial tensile stress field; Second stage-The transition of tensile stress field; Third stage-In control of circumferential tensile stress field; Fourth stage-Becoming uniform stress field.

5.1.1. First stage (60 μs–150 μs)

750 g TNT charge is ignited at $t = 0$ μs. Because of the same standoff distance, the blast loading begins to interact with the square plate and cylindrical shell on material around the center hole at the same time $t = 60$ μs. As shown at t = 110 μs, before the blast loading arriving at the cover plate, the stress-zone generated by the blast loading occurs on the square plate with a circular shape while on the cylindrical shell with a shape similar to rectangle, which is due to the geometrical difference of cylindrical shell between axial and circumferential direction. In addition, the stress concentration zone of square plate is uniformly distributed around the center hole, however, because of blast loading firstly arriving at middle line of cylindrical shell in axial direction, the stress concentration zone of cylindrical shell is only shown along axial direction around the center hole. As shown at $t = 150$ μs, after arriving at the cover plate, with the blast loading acting on these two structures progressively, the stress-zone on the square plate is represented as a shape similar to rectangle covering up all holes exactly, at the same time, the zones of reflected stress appear near the cover plate. There is a significant stress concentration zone around the center hole and there are eight relatively week stress concentration zones between other adjacent holes. For cylindrical shell, the loading area is covered with stress-zone completely. The stress concentration zones appear on the regions of non-holes along circumferential direction and the regions between holes along axial direction, as a result, there are two stress concentration bands along circumferential direction between three rows of holes. This phenomenon can be attributed to the generating of plastic hinge along circumferential direction more easy than that along axial direction because of the arc configuration and the existence of pre-formed holes, therefore, the axial tensile stress field is generated and broken off by holes.

5.1.2. Second stage (150 μs–290 μs)

From $t = 150$ μs to $t = 210$ μs, the stress concentration zone of square plate is changing to the region between the center hole and the outer holes. However, with the deforming downwards, the intensity of the circumferential tensile stress field increases quickly and the global tensile stress filed comes into the stage of transition. Accordingly, the stress concentration zones of cylindrical shell are distributed between the adjacent holes and between holes and the cover plate along axial direction, at the same time, stress on the region of non-holes along axial direction begins to dissipate, as

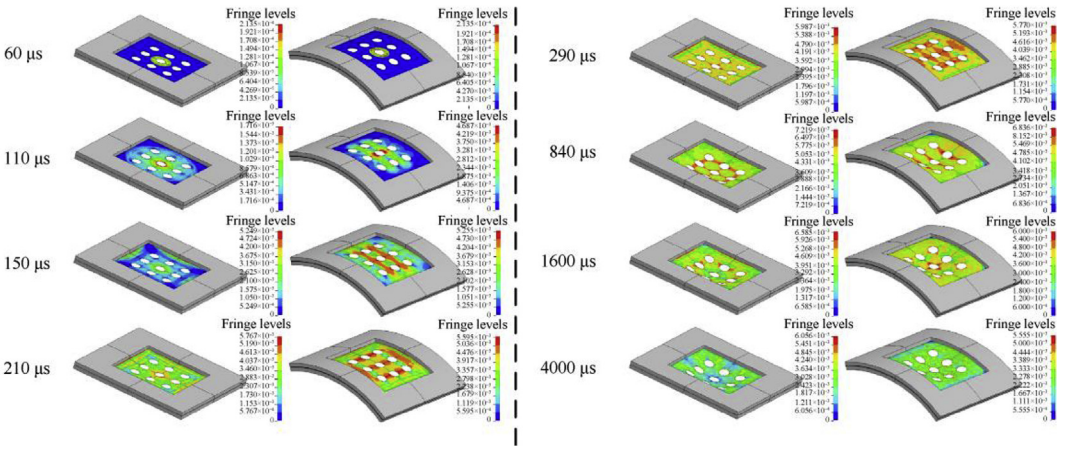

Fig. 11. The structure response process and stress field of square plate and cylindrical shell with pre-formed circular holes under blast loading.

Please cite this article as: Li W et al., The deformation and failure mechanism of cylindrical shell and square plate with pre-formed holes under blast loading, Defence Technology, https://doi.org/10.1016/j.dt.2020.06.014

shown at $t = 210$ μs. As a result, there are three stress concentration bands along axial direction and broken by holes. As demonstrated at $t = 290$ μs, the stress concentration zones of square plate change to the nine regions around nine hole, respectively. However, with cylindrical shell deforming downwards progressively, the axial tensile stress field is being translating to the circumferential tensile stress field, consequently, the middle stress concentration band along axial direction is becoming to extent along circumferential direction until intersecting with the other two stress concentration bands along axial direction.

5.1.3. Third stage (290 μs–840 μs)

From $t = 290$ μs to $t = 840$ μs, a global sunken deformation with a circular shape tending to square shape is generated for the square plate, while that with an elliptical shape tending to square shape is generated for the cylindrical shell. This is an interesting trend because of the existence of pre-formed holes. As shown at $t = 840$ μs, the stress concentration zone of square plate is located at the region between the adjacent holes and the intensity of the stress concentration zone between outer holes is bigger relatively. The stress concentration zone of cylindrical shell is only located between holes along circumferential direction, which indicates that this stage has been in control of circumferential tensile stress field.

5.1.4. Forth stage (840 μs–4000 μs)

From $t = 840$ μs to $t = 1600$ μs, with the global sunken deformation increasing rapidly, the intensity of stress concentration is dissipating due to the energy of blast loading translating to the energy of plastic deformation. The stress concentration zone is only around the holes in a small range at $t = 1600$ μs and disappears completely at $t = 4000$ μs, which indicates that this stage has been in control of uniform stress field.

5.2. The local and global deformation curves

The same configuration, parameters, blast loading, boundary and mesh method as Figs. 1 and 9 but without the pre-formed holes are adopted as the control experiment performed by the method of numerical simulation. A typical displacement time histories at the max-deformation point of the square plate and cylindrical shell with and without pre-formed holes are given in Fig. 12 the peak deformation of cylindrical shell and square plate with pre-formed holes are 73.9 mm and 61.5 mm,in addition, the permanent deformation of cylindrical shell and square plate with pre-formed holes are 70.5 mm and 58.7 mm, while the peak deformation of cylindrical shell and square plate without pre-formed holes are 65.3 mm and 52.7 mm, besides, the permanent deformation of cylindrical shell and square plate with pre-formed holes are 61.9 mm and 47.8 mm, that is, the peak and permanent displacement of the cylindrical shell with pre-formed holes are 13.2% and 13.9% more than that without pre-formed holes, likewise, the peak and permanent displacement of the square plate with pre-formed holes are 16.7% and 22.8% more than that without pre-formed holes, which indicates that the square plates have a better performance than that of cylindrical shell with or without pre-formed holes, whereas the influence of pre-formed holes on the reduction of blast-resistant capability of square plate is bigger than that of cylindrical shell. This may be caused by being in control of single direction tensile stress field for the cylindrical shell, while all direction tensile stress field for the square plate, as described at section 4.1. Because of the local deformation occurring around the circular holes, it is not enough to comprehensively describe the deformation by comparing the displacement time histories at the max-deformation point. For demonstrating the difference of the local deformation between these two structures with pre-formed holes, the permanent deformation curves at the center locus and 1/4 locus of them as shown in Fig. 13. In addition, the center and 1/4 locus are considered in axial and circumferential direction of cylindrical shell, respectively, on account of the difference of curves between these two directions.

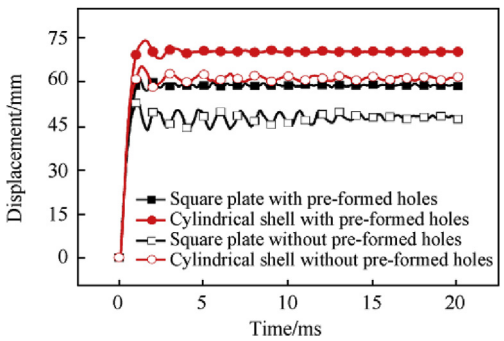

Fig. 12. Comparison of displacement time histories at the max-deformation point between the square plate and cylindrical shell.

Fig. 13 shows the permanent local deformation at the center locus and 1/4 locus of the square plate and cylindrical shell. As shown in Fig. 13 for the center zone of these two structures, the maximum and minimum local deformation at the center locus are belong to cylindrical shell along axial direction and square plate, respectively, however, that at the 1/4 locus are belong to cylindrical shell along circumferential direction and square plate, respectively. For the zone near the cover plate, the maximum and minimum local deformation at the center locus are belong to cylindrical shell along axial direction and cylindrical shell along circumferential direction, respectively, which is the same as that at the 1/4 locus. This phenomenon of local deformation indicates that the local deformation of cylindrical shell is bigger than that of square plate for a majority of zones besides the zone along the circumferential direction near the cover plate. Comparing Fig. 13(a) and (b), the deformation of square plate at the center locus is bigger than that at the 1/4 locus, which indicates that a local sunken with an approximate spherical surface has been generated and the center hole keeps a circular shape. In addition, the deformation of cylindrical shell along axial direction at the center locus is bigger than that at the 1/4 locus, however, there is almost no difference between the deformation of cylindrical shell along circumferential direction at the center locus and the 1/4 locus, which indicates that the shape of the center hole is similar to a space shape of saddle.

In order to explore the reason leading to the phenomena above, the existence of pre-formed holes and the different configuration of cylindrical shell between the axial direction and the circumferential direction are presented in this study as two viewpoints. The local deformation between the square plate and cylindrical shell with pre-formed holes is shown in Fig. 14, which has the same phenomena as the cylindrical shell and square plate with pre-formed holes and indicates that the different configuration of cylindrical shell between the axial direction and the circumferential direction is key leading to the phenomena mentioned above and the existence of pre-formed holes just has an effect to increase the global and local deformation. Besides, the comparison of the phenomena between Figs. 13 and 14 also indicates the smoothness of space surface of cylindrical shell and square plate after permanent deformation, otherwise the shape of wave would appear on them. Comparing Figs. 13(a) and Fig. 14(a), there is an interesting phenomenon that the shape of the curve between the center hole and the adjacent holes at the center locus along axial or circumferential direction is raised towards the source of TNT charge for cylindrical

Please cite this article as: Li W et al., The deformation and failure mechanism of cylindrical shell and square plate with pre-formed holes under blast loading, Defence Technology, https://doi.org/10.1016/j.dt.2020.06.014

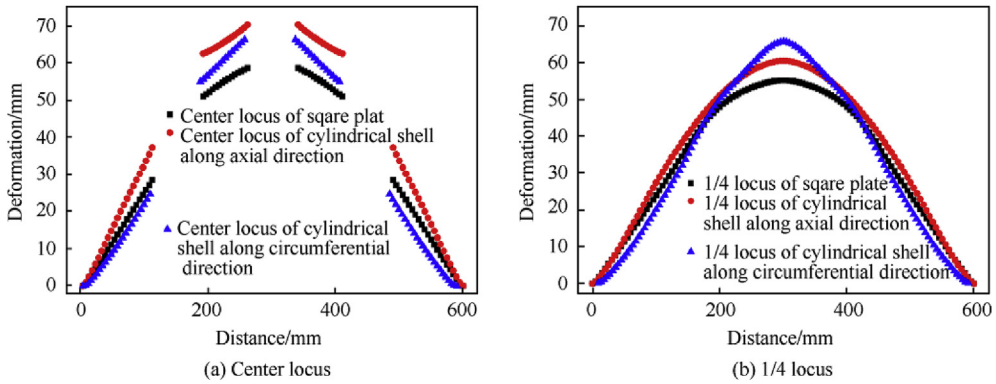

Fig. 13. The local deformation between the square plate and cylindrical shell with pre-formed holes.

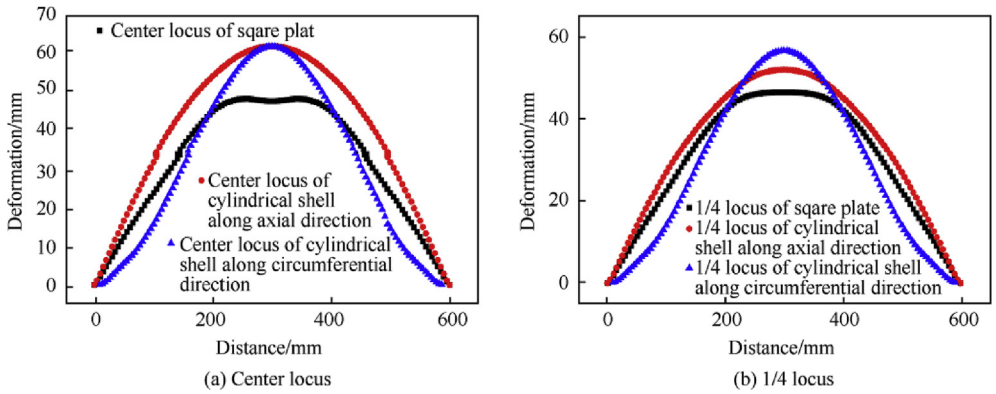

Fig. 14. The local deformation between the square plate and cylindrical shell without pre-formed holes.

shell with pre-formed holes, however this phenomenon is not existent for cylindrical shell without preformed holes and for square with or without preformed holes, which may result from the combination of the local effect of pre-formed holes and the different configuration of cylindrical shell between the axial direction and the circumferential direction.

5.3. Degree of damage at typical points

According to the structure response process, the distributing of stress concentration and failure mode studied in section 4.1 and 4.6, the typical points is chosen at the edge of pre-formed holes in order to analyze the degree of damage and marked from "*A*" to "*E*" as shown in Fig. 15. Because of the different configuration along axial and circumferential direction of cylindrical shell, the subscript "0", "1" and "2" are defined to represent the typical points on the square plate, along axial and circumferential direction of cylindrical shell, respectively. The rule of the subscript will be used in section 4.3-4.5.

As shown in Fig. 16, the degree of damage at five typical points is defined as the damage factor D in Eqs. (2) and (3). When the damage factor D reaches 1, the material fails and the crack will be generated and propagating. The operating condition in the simulation were that 750 g TNT charge and 250 mm standoff distance. Fig. 16(a)–(e) shows the damage factor history at point *A*-*E* series on square plate and cylindrical shell. The damage factor history curve can be divided into three stage: elastic deformation, plastic accumulation, keeping constant. The earliest point comes into the stage of plastic accumulation is point A_1, B_1, C_1, D_2 and E_2, which indicates that the configure difference of cylindrical shell between axial and circumferential direction easily leads to unequally distributed deformation relative to square plate at the forepart of deformation. In addition, the line between point A_1, B_1, and C_1 is along axial direction and the line between D_2 and E_2 is also along

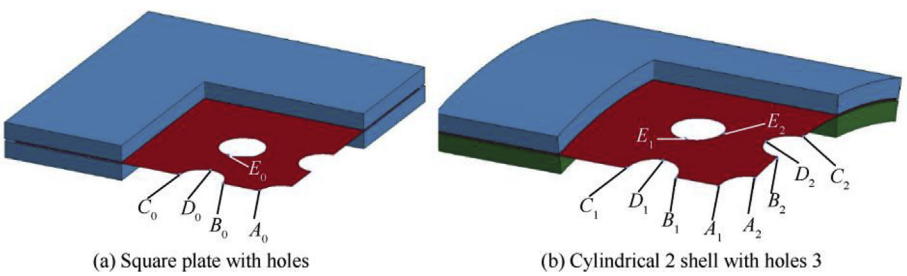

Fig. 15. The typical points for analyzing the degree of damage.

Please cite this article as: Li W et al., The deformation and failure mechanism of cylindrical shell and square plate with pre-formed holes under blast loading, Defence Technology, https://doi.org/10.1016/j.dt.2020.06.014

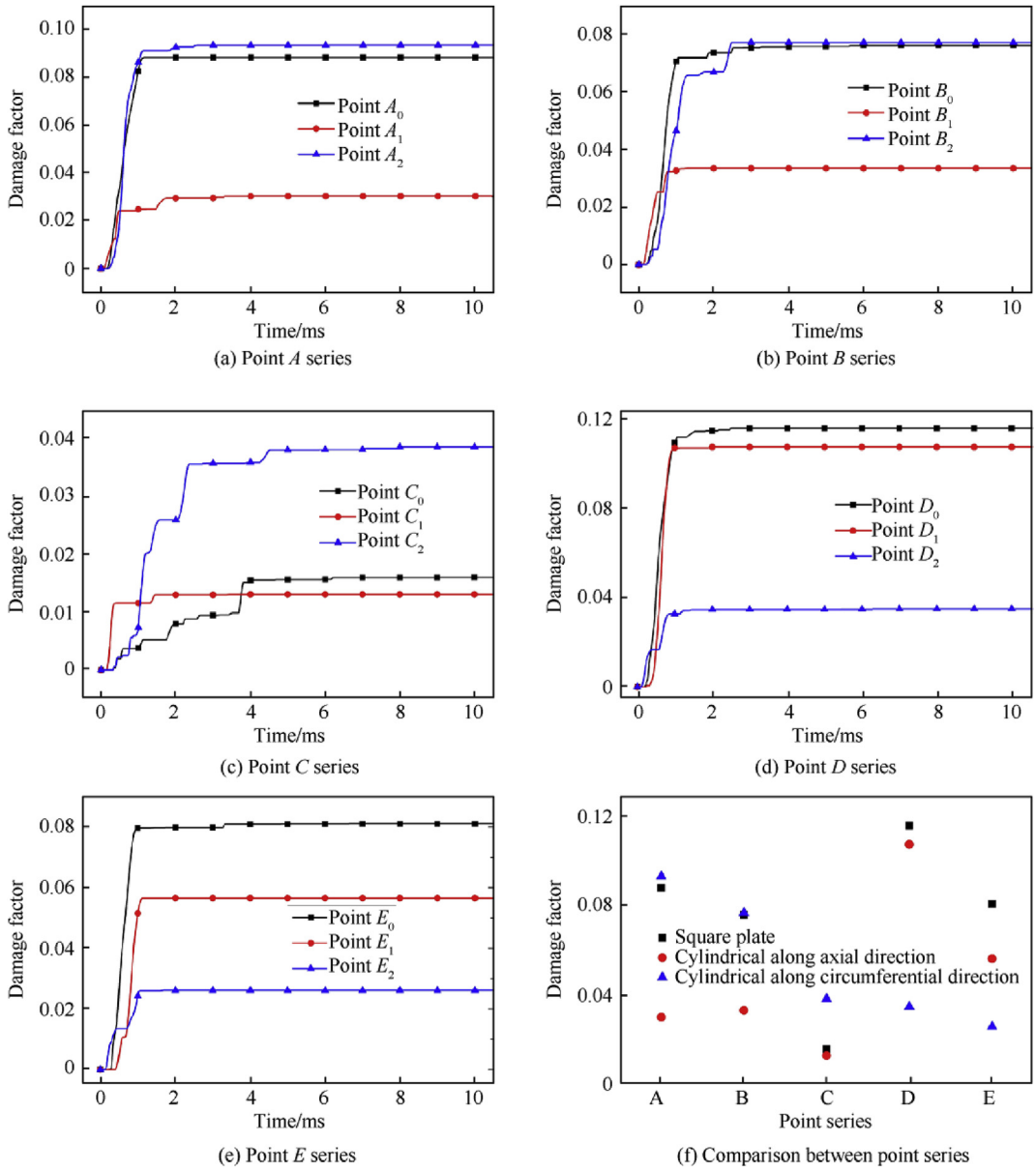

Fig. 16. The comparison of damage factor at five typical points between square plate and cylindrical shell with pre-formed holes.

axial direction, which indicates that the plastic deformation begins along axial direction of cylindrical shell and corresponds to the phenomenon mentioned in section 4.1.1. The damage factor history curve of these five point series interlace with each other in the stage of plastic accumulation, which exhibits the transition of tensile stress field in manner of damage changing and corresponds with the description in second stage of structure response process. The damage factor history curves at point *A*, *D* and *E* series reach the stage of keeping constant at about 1 ms earlier than that at point *B* and *C* series at about 2.5 ms–4.5 ms. The final damage factor at point *A*-*E* series are listed in Table 2 and shown as Fig. 16(f), it can be seen that the degree of damage at point *A* and *B* on square plate is similar to that on cylindrical shell along circumferential direction and larger than that on cylindrical shell along axial direction, and the degree of damage at point *C* on square plate is similar to that on cylindrical shell along axial direction and smaller than that on cylindrical shell along circumferential direction, while the largest and smallest degree of damage at point *D* and *E* are both on square plate and on cylindrical shell along circumferential direction, respectively, which indicates that when the standoff distance of 750 g TNT charge is 250 mm, the failure of square plate and cylindrical shell with pre-formed holes easily appears at point *D* and *E* series, and this suppose has been validated in section 4.6.

Table 2
The final damage factor of typical points.

Series	*A*	*B*	*C*	*D*	*E*
Subscript "0"	0.088	0.076	0.016	0.116	0.081
Subscript "1"	0.030	0.033	0.013	0.108	0.057
Subscript "2"	0.093	0.077	0.039	0.035	0.027

5.4. Dynamic stress concentration at typical points

Although the phenomenon and transformation of stress concentration has been observed in Fig. 11 and discussed in section 4.1,

Please cite this article as: Li W et al., The deformation and failure mechanism of cylindrical shell and square plate with pre-formed holes under blast loading, Defence Technology, https://doi.org/10.1016/j.dt.2020.06.014

it is still necessary to obtain the quantitative analysis of stress concentration in order to investigate and compare the influence of pre-formed holes on the blast-resistance between square plate and cylindrical shell. The dynamic stress concentration factor $K_d(t)$ is adopted to represent the influence of pre-formed holes at any moment t and defined as Eq. (6), [13].

$$K_d(t) = \sigma_{dw}(t)/\sigma_{dn}(t) \tag{6}$$

where $\sigma_{dw}(t)$ is the dynamic stress of structures with pre-formed holes at any moment t, $\sigma_{dn}(t)$ is the dynamic stress of structures without pre-formed holes at any moment t.

The operating condition in the simulation were that 750 g TNT charge and 250 mm standoff distance. Fig. 17(a)–(e) shows the dynamic stress concentration factor history(the solid line) and the integral curve(the dash line) at five typical point A-E series on square plate and cylindrical shell which have been mentioned in section 4.3. At the initial moment, the max dynamic stress concentration factor appears at the point A_1-D_1 and E_2 and reaches 1.9, 3.5, 3.1, 2.2 and 3.6, respectively. Afterwards, the peak value of dynamic stress concentration factor appears obviously after 1.6 ms at all point series and reaches 5.1, 5.9, 4.4, 5.5 and 3.9, respectively. In addition, from the initial moment to 1.6 ms, the dynamic stress concentration factor is below 2 with slight fluctuation. However, the stress concentration zone begins to disappear after 1.6 ms and the stress field becomes into the control of uniform stress field with large deformation, which has been observed and mentioned in section 4.1. Accordingly, it can be concluded that there is a small influence of pre-formed holes on dynamic stress concentration at the stages with sharp change of stress fields(from First stage to Third stage mentioned in section 4.1), while a great influence of pre-formed holes on dynamic stress concentration at the stage with uniform stress field(Forth stage mentioned in section 4.1), which indicates that the difference in large deformation

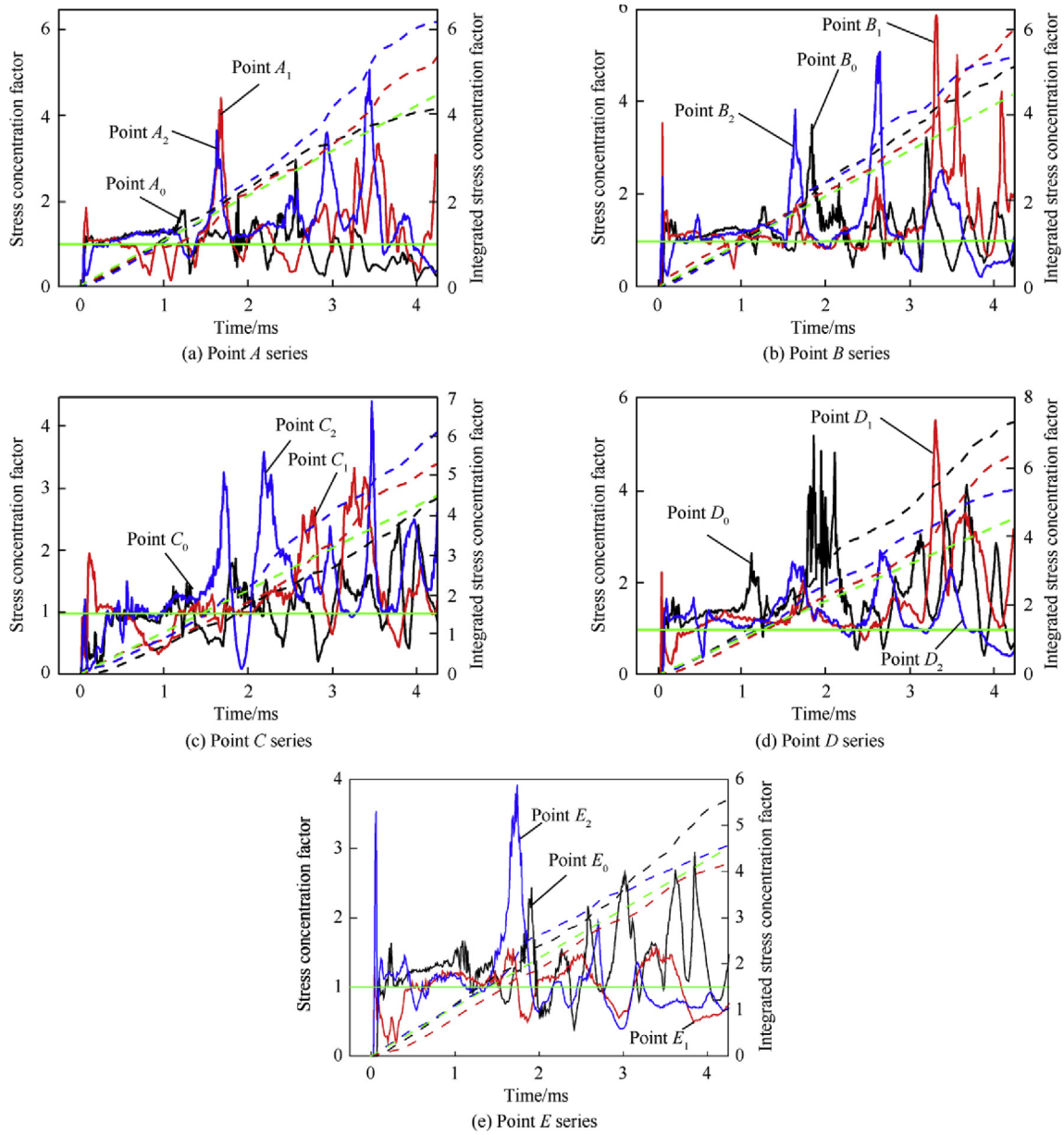

Fig. 17. The comparison of dynamic stress concentration factor at five typical points between square plate and cylindrical shell with pre-formed holes.

Please cite this article as: Li W et al., The deformation and failure mechanism of cylindrical shell and square plate with pre-formed holes under blast loading, Defence Technology, https://doi.org/10.1016/j.dt.2020.06.014

between with and without the pre-formed holes is the key to the influence on degree of stress concentration.

As shown in Fig. 17, the dynamic stress concentration factor history curves all fluctuate nearby the value of 1(the green solid line), which indicates that the existence of pre-formed holes not only lead to the increasing of stress concentration around the holes, but also release the stress concentration. In order to express the total contribution of stress concentration and stress dissipation due to pre-formed holes, The Integrated dynamic stress concentration factor $I_{kd}(t)$ at any moment t was defined as Eq. (7).

$$I_{kd}(t) = \int_0^t K_d(t)\mathrm{d}t \tag{7}$$

where $K_d(t)$ is the dynamic stress concentration factor at any moment t and defined as Eq. (6).

As shown in Fig. 17(a)–(e), the green dash line is the integration of the green solid line and represents the total contribution that stress concentration and stress dissipation balance out. For point B and D series, the integrated dynamic stress concentration factor curves of all points are above the green dash line. For point A and C series, the integrated dynamic stress concentration factor curves of points on square plate are below the green dash line and that of points on cylindrical shell are above. For point E series, the integrated dynamic stress concentration factor curve of point along axial direction of cylindrical shell is below the green dash line. It can be concluded that the total contribution of stress concentration and stress dissipation due to pre-formed holes at the points A_0、C_0 and E_1 are tenting to status of stress dissipation and others are tenting to status of stress concentration, which indicates that the status of stress concentration and stress dissipation occur around the pre-formed holes of the square plate and cylindrical shell, simultaneity.

5.5. Change of stress status at typical points

In order to study and compare the influence of pre-formed holes on the ductile fracture between square plate and cylindrical shell, the stress status change is analyzed and discussed. The value of stress triaxiality η and the deviatoric state parameter ξ can be used to describe the material stress status and can correspond to the stress status one by one as listed in Table 3 [24–27], which are defined as Eqs. (8) and (9). And the fracture strain decreases with increasing of stress triaxiality [28].

$$\eta = \frac{\sigma_1 + \sigma_2 + \sigma_3}{3\sqrt{\frac{1}{2}\left[(\sigma_1 - \sigma_2)^2 + (\sigma_2 - \sigma_3)^2 + (\sigma_3 - \sigma_1)^2\right]}} \tag{8}$$

$$\xi = -\frac{27}{2}\eta\left(\eta^2 - \frac{1}{3}\right) \tag{9}$$

Where σ_1, σ_2 and σ_3 are the principle stresses. Because of the relationship of Eq. (9) between the stress triaxiality η and the deviatoric state parameter ξ, as a matter of convenience, the stress triaxiality η is adopted as one and only parameter to analyze and discuss the stress status change.

Table 3
The relationship between stress triaxiality and the stress status.

Stress status	Stress triaxiality η
Pure pressure	~ −0.33
From pure pressure to pure shear	−0.33 ~ 0
Pure shear	0
From pure shear to pure tentile	0–0.33
Pure tentile	0.33~

The operating condition in the simulation were that 750 g TNT charge and 250 mm standoff distance. Fig. 18(a)–(e) shows the stress triaxialality history at five typical point *A-E* series on square plate and cylindrical shell which have been mentioned in section 4.3. At the initial stage (0 ms–0.5 ms), namely, before Third stage mentioned in section 4.1, the stress state of typical points on cylindrical shell reciprocate sharply between the pure pressure and pure tentile, while that on square plate keep the pure tentile or reciprocate between pure tentile and pure shear, which indicates that the square plate fractures more easier than cylindrical shell at the typical point series around the pre-formed holes at the initial moment. At the stage from 0.5 ms to 1.2 ms, namely between Third stage and Fourth stage mentioned in section 4.1, the stress triaxiality curves of a majority of typical point *A-E* series fluctuate nearby the value of 0.33, except that of the point C_1 reciprocate between −0.33 and 0 and that of the point A_1 and B_1 reciprocate between 0 and 0.33 from 0.8 ms to 1.2 ms, which exhibits the transition of tensile stress field in manner of stress status changing and also indicates that the fracture happens mainly at this stage. At the stage from 1.2 ms to 2.5 ms, namely Fourth stage in section 4.1, the stress state of typical points A-E series fluctuate between pure tentile and pure pressure with one or two wavelength, which is due to the free oscillation of these two kinds of structures with almost permanent deformation.

5.6. Failure modes and crack propagation process

In order to obtain the failure modes, crack propagation process and the critical equivalent TNT value(the minimal equivalent TNT value when failure occurs), the standoff distance of 100 mm, 150 mm, 250 mm, 300 mm, 400 mm and 500 mm are selected to detonate the charge, in addition, the adaptive mesh refinement and element erosion are adopted to present the crack propagation on the plate and shell [15].

In order to obtain the critical equivalent TNT value with a certain standoff distance, the mass of TNT charge is gradually increased 100 g by 100 g until failure occurred on the square plate and the cylindrical shell. As listed in Table 4, the critical equivalent TNT value have been obtained with standoff distance from 100 mm to 500 mm. At the standoff distance of 100 mm,the critical equivalent TNT value applied on square plate is equal to that on cylindrical shell. At the standoff distance from 150 mm to 400 mm, the critical equivalent TNT value applied on cylindrical shell is 10%, 6.7%, 5.6% and 8% smaller than that on square plate. While, at the standoff distance of 500 mm, the critical equivalent TNT value applied on cylindrical shell is 10% bigger than that on square plate. The tendency above indicates that cylindrical shell provides a better performance of blast-resistance than square plate at a bigger standoff distance, comparing that at a smaller standoff distance, which may be attributed to that the cylindrical shell is in control of single direction tensile stress field at a smaller standoff distance due to the geometrical characteristic of arch configuration while in control of relative uniform stress field at a bigger standoff distance.

As shown in Fig. 19, the shapes of fracture under the critical equivalent TNT value corresponding to the different standoff distance are obtained and are classified as three(S1, S2 and S3) and two(C1 and C2) kinds of failure modes for square plate and cylindrical shell with pre-formed holes, respectively. That is, the failure mode S1(standoff distance from 100 mm to 150 mm)- fracture of the center hole; the failure mode S2(standoff distance from 250 mm to 300 mm)- fracture of the outer holes; the failure mode S3(standoff distance from 400 mm to 500 mm)- fracture of the

Please cite this article as: Li W et al., The deformation and failure mechanism of cylindrical shell and square plate with pre-formed holes under blast loading, Defence Technology, https://doi.org/10.1016/j.dt.2020.06.014

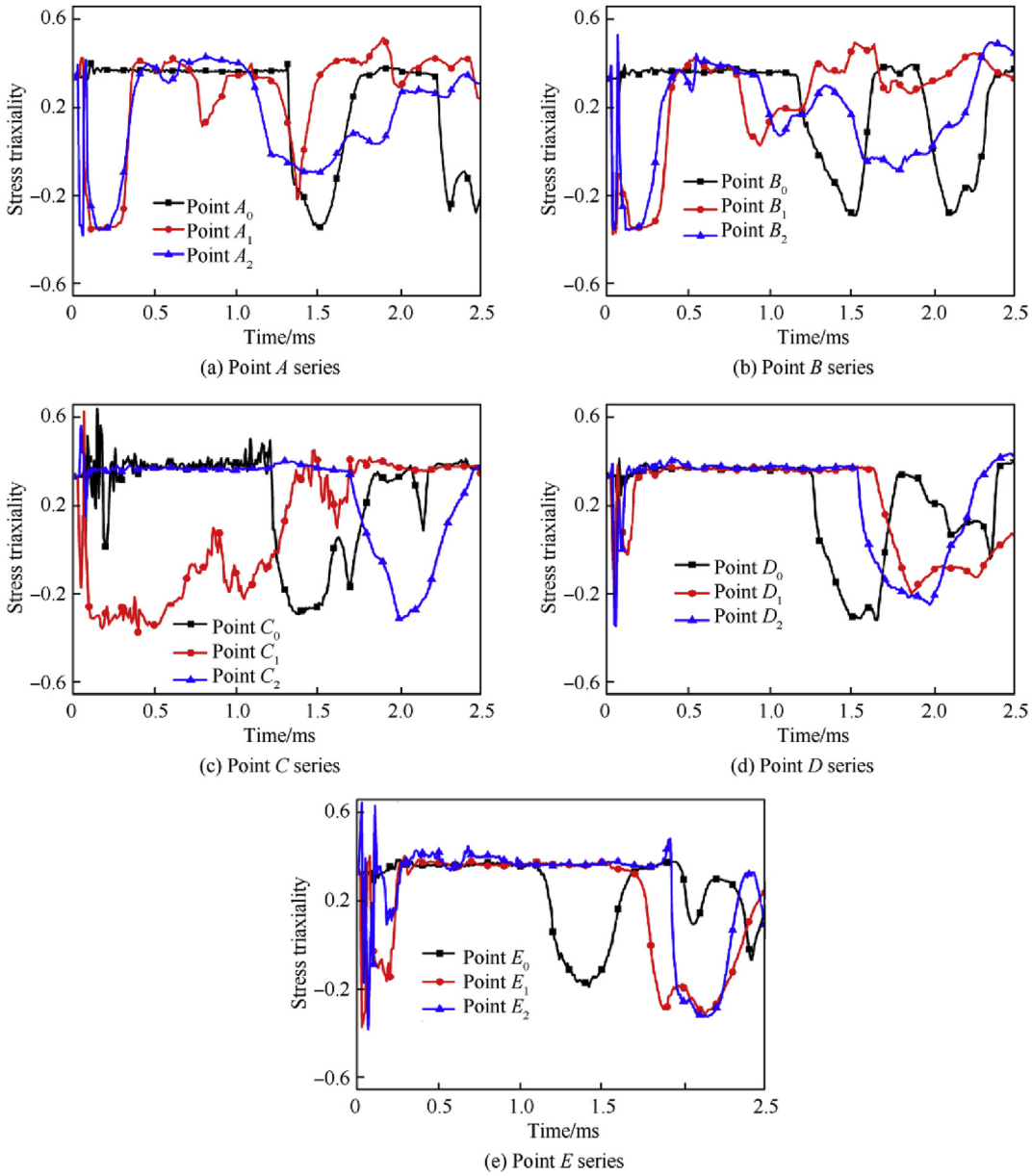

Fig. 18. The comparison of stress status change at five typical points between square plate and cylindrical shell with pre-formed holes.

Table 4
The critical equivalent TNT value.

Standoff distance	100 mm	150 mm	250 mm	300 mm	400 mm	500 mm
Square plate	500 g	1000 g	1500 g	1800 g	2500 g	3000 g
Cylindrical shell	500 g	900 g	1400 g	1700 g	2300 g	3300 g
Reduction	0%	10%	6.7%	5.6%	8%	−10%

boundary; the failure mode C1(standoff distance from 100 mm to 150 mm)- fracture of the midline holes along circumferential direction and the failure mode C2(standoff distance from 250 mm to 500 mm)- fracture of the side holes along circumferential direction. Although the fracture shapes of the cylindrical shell at the standoff distance from 250 mm to 500 mm all belong to the same failure mode C2, the degree of fracture decreases with the increasing of standoff distance. Considering the influence of blast intensity on the failure modes, some events with gradual value of TNT charge above the critical equivalent TNT value for every standoff distance have been performed and compared, it can be concluded that the blast intensity has an influence on the degree of fracture and failure but not on failure modes.

In order to analyze the crack propagation of different failure modes, an event has been chosen from every failure mode and the process of the crack propagation has been shown in Fig. 20 and Fig. 21. For failure mode S1 (standoff distance of 100 mm and under 500 g TNT), cracks initiate at the point A_0 mentioned in section 4.3

Please cite this article as: Li W et al., The deformation and failure mechanism of cylindrical shell and square plate with pre-formed holes under blast loading, Defence Technology, https://doi.org/10.1016/j.dt.2020.06.014

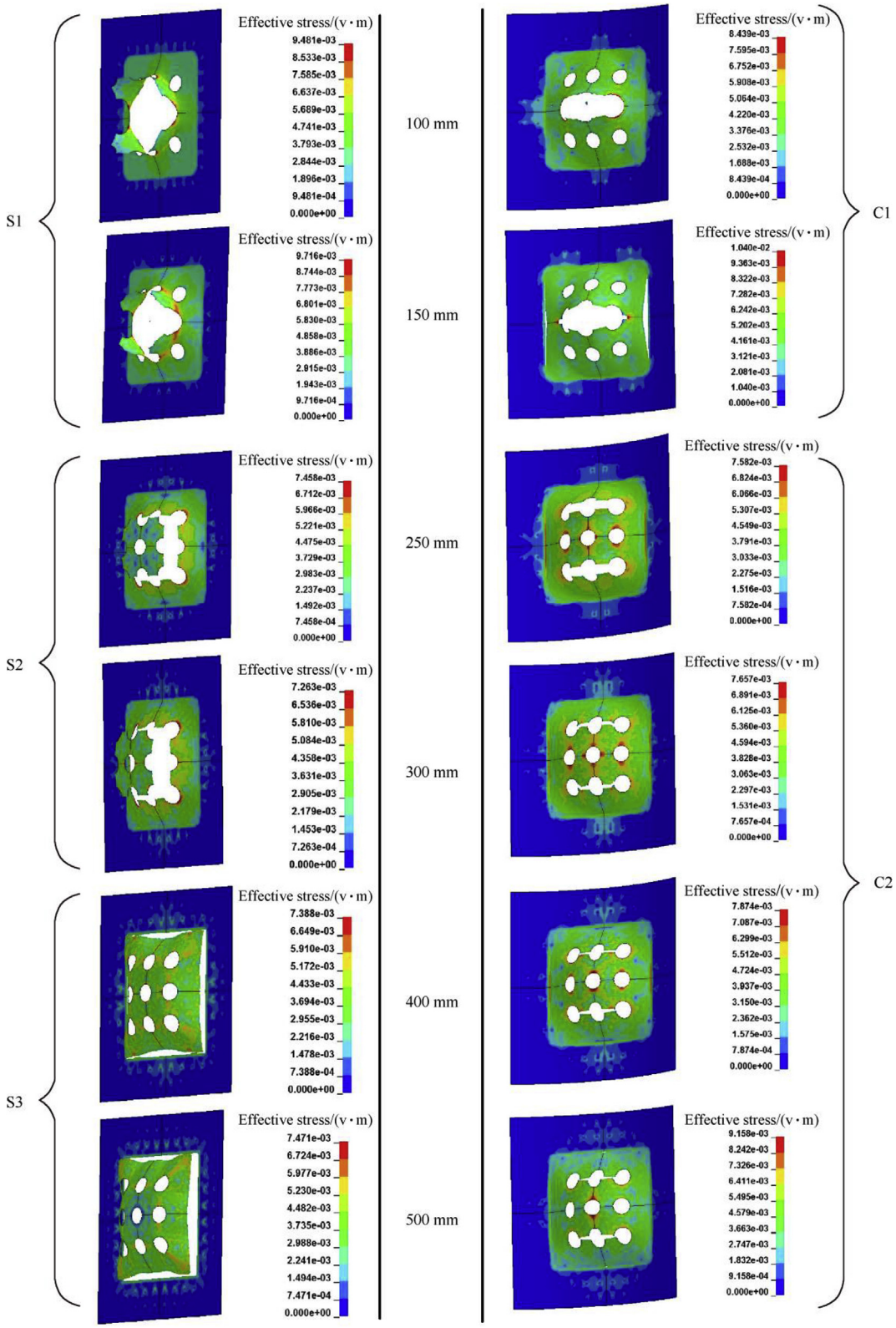

Fig. 19. The comparison of failure mode between cylindrical shell and square plate with pre-formed circular holes.

and propagate along the line(A_0B_0) between the adjacent holes until run-through, subsequently, the petal-like broken hole is formed and expanded outwards. For failure mode S2 (standoff distance of 250 mm and under 1500 g TNT), cracks initiate at the point D_0 and propagate along the line(D_0E_0) between the adjacent holes until run-through, subsequently, the square-like plate with the center hole is perfectly separated from the original structure and flying towards the direction of blast loading. For failure mode

Please cite this article as: Li W et al., The deformation and failure mechanism of cylindrical shell and square plate with pre-formed holes under blast loading, Defence Technology, https://doi.org/10.1016/j.dt.2020.06.014

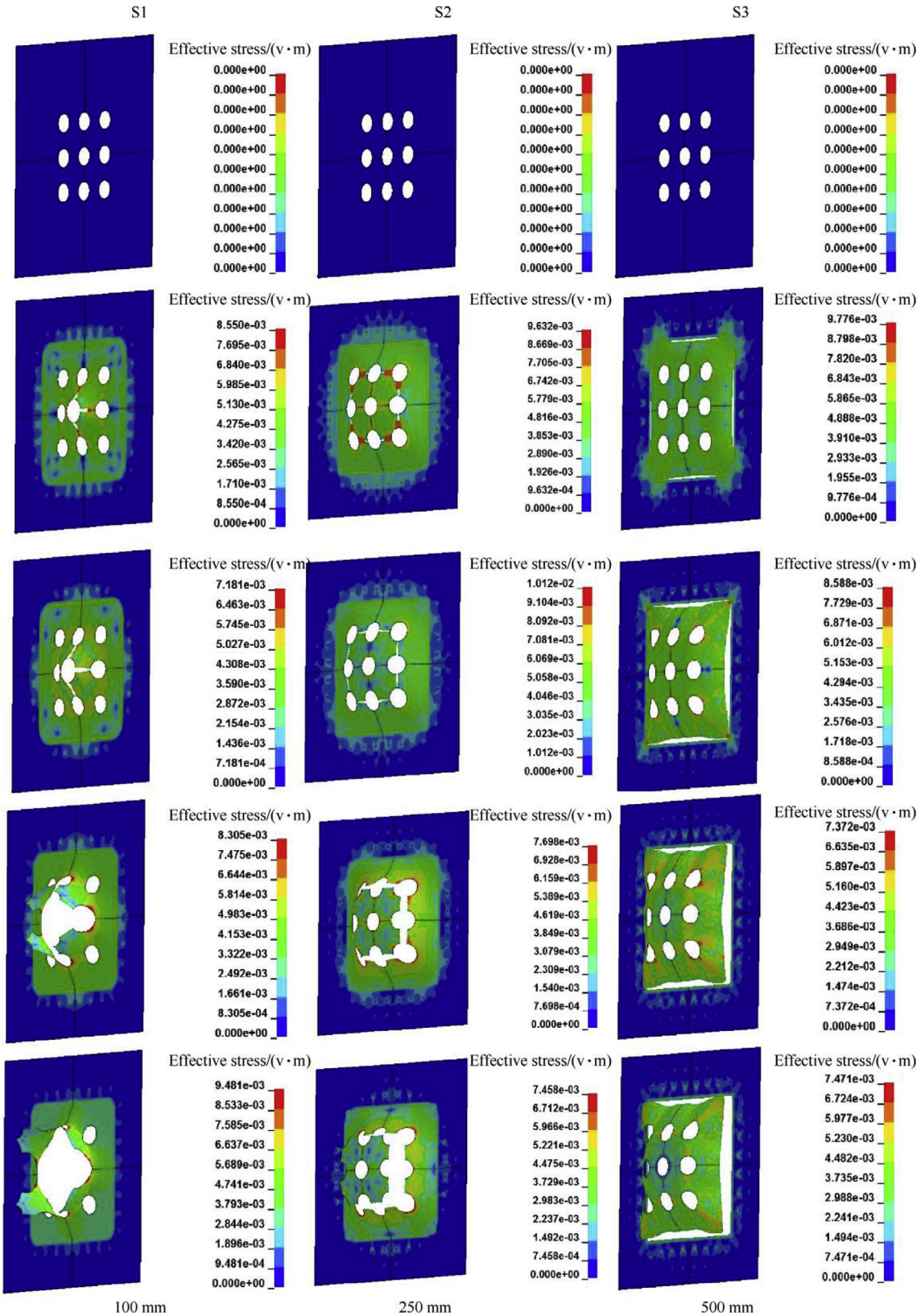

Fig. 20. The crack propagation of different failure modes for square plate with circular holes.

Please cite this article as: Li W et al., The deformation and failure mechanism of cylindrical shell and square plate with pre-formed holes under blast loading, Defence Technology, https://doi.org/10.1016/j.dt.2020.06.014

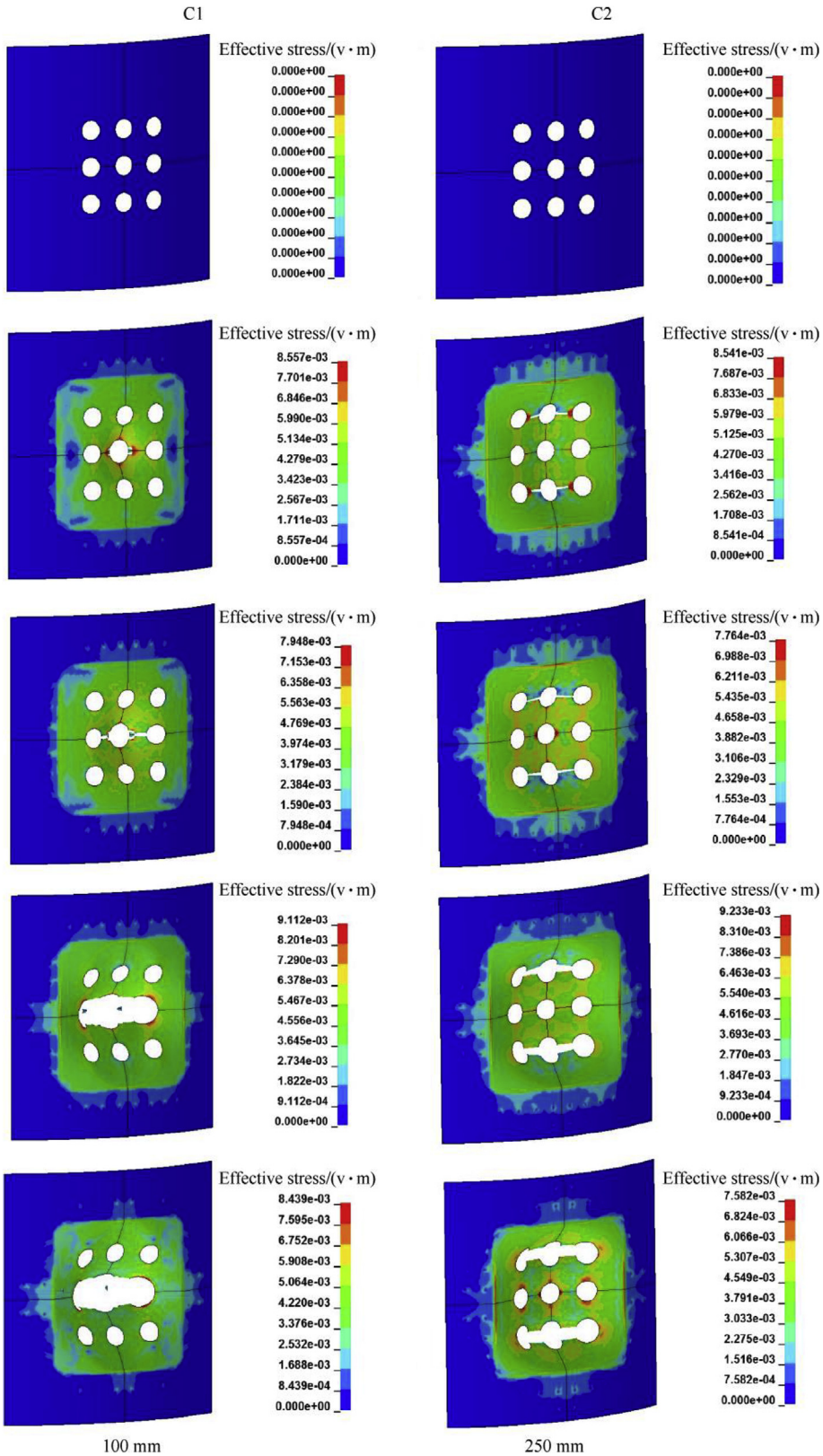

Fig. 21. The crack propagation of different failure modes for cylindrical shell with circular holes.

Please cite this article as: Li W et al., The deformation and failure mechanism of cylindrical shell and square plate with pre-formed holes under blast loading, Defence Technology, https://doi.org/10.1016/j.dt.2020.06.014

S3 (standoff distance of 500 m m and under 3000 g TNT), cracks initiate at the midpoint of the inner boundary of the cover plate and propagate along this boundary until intersecting with each other, subsequently, the entire loading area is separated from the cover plate and flying towards the direction of blast loading. For failure mode C1 (standoff distance of 100 mm and under 500 g TNT), cracks initiate at the point A_2 mentioned in section 4.3 and propagate along the line(A_2B_2) between the adjacent holes until run-through, subsequently, the elliptic broken hole is formed by linking the three holes along circumferential direction and expanded outwards. For failure mode C2 (standoff distance of 250 mm and under 1400 g TNT), cracks initiate at the point D_1 mentioned in section 4.3 and propagate along the line(D_1E_1) between the adjacent holes until run-through, subsequently, two elliptic broken holes are formed by linking the three holes along circumferential direction and expanded outwards. According to the stress nephogram shown in Figs. 20 and 21 and the discussion in section 4.4, the crack initiation points and the edges of the crack in the propagation path mentioned above are both the locations of stress concentration, which contributes to the failure.

According to the failure modes and the process of crack propagation described above, there are two conclusions obtained as follows: On one hand, the point at which the crack initiates is further from the center of structure with the standoff distance increasing, which is because the time sequence and the space distributing of the shock wave applied on each parts of structure are different and decided by the standoff distance and have a key influence on the forming location of the crack initiating point and the locus of crack propagation; On the other hand, comparing the failure modes under different standoff distance between square plate and cylindrical shell, the local fracture/failure mode appears on both square plate and cylindrical shell at a smaller standoff distance from 100 mm to 150 mm. With increasing of standoff distance, there are two kinds of failure modes appearing on the square plate at the standoff distance from 250 mm to 300 mm and from 400 mm to 500 mm, respectively, however, there is only one kind of failure modes appearing on the cylindrical shell at the standoff distance from 250 mm to 500 mm, which may be attributed to that the generating of plastic hinge along circumferential direction of cylindrical shell is more easy than that along axial direction because of the arc configuration of cylindrical shell and the existence of pre-formed holes. Accordingly, the occurring of crack initiating point at point D_1 and the crack propagation along the locus of D_1E_1(axial direction) are more easy than other points and locus, after crack run through the adjacent holes, the stress concentration zone along circumferential direction and near the cover plate will dissipate and there will be no more cracks occurring on the cylindrical shell.

6. Conclusion

This study presents the deformation and failure mechanism of cylindrical shells and square plate considering the influence of pre-formed holes under blast loading by employing a numerical model validated. The structure response and stress field changing process has been divided into four specific stages from the viewpoint of stress concentration and the deformation mechanism has been discussed systematically. The local and global deformation curves, degree of damage, change of stress status and failure modes of cylindrical shell and square plate with pre-formed circular holes under blast loading are obtained, compared and analyzed, it can be concluded as: (1) The transition of tensile stress fields is due to the geometrical characteristic of pre-formed holes and cylindrical shell with arch configuration and is demonstrated by damage factor and stress triaxialality; (2) Comparing with structures without pre-formed holes, the existence of pre-formed holes not only lead to the increasing of stress concentration around the holes, but also release the stress concentration during whole response process; (3) There are three and two kinds of failure modes for square plate and cylindrical shell with pre-formed holes, respectively. and the standoff distance has a key influence on the forming location of the crack initiating point and the locus of crack propagation; (4) The square plates with pre-formed holes has a better performance than cylindrical shell on blast-resistant capability at a smaller standoff distance, while the influence of pre-formed holes on the reduction of blast-resistant capability of square plate is bigger than that of cylindrical shell, which may be mainly due to the geometrical characteristic of cylindrical shell with arch configuration. Because of the multiformity of fragment perforation distributing and number, to obtain the deformation and failure mechanism at a much wider range, we need to investigate further on the influence of the number and distribution of pre-formed holes in our subsequent research.

Declaration of competing interest

We declare there is no competing interest.

Acknowledgments

The reported research is financially supported by The National Natural Science Foundation of China under Grant No.11902310 and No. 11802292. The financial contributions are gratefully acknowledged.

References

[1] Forsén R, Nordström M. Damage to reinforced concrete slabs due to the combination of blast and fragment loading, PS Bulson, vol. 139. London: Thomas Telford; 1992.
[2] He X, Pang W, Qu J, Liu G, Li M. Protective door damaged by air shock wave and fragment arisen from explosion in prototype tunnel. Explos Shock Waves 2004;5:475–9.
[3] Nystrom U, Gylltoft K. Numerical studies of the combined effects of blast and fragment loading [J]. Int J Impact Eng 2009;36:995–1005.
[4] Zhang C, Zhu X, Hou H, Chen C. Tests for combined damage effect of blast waves and high-velocity fragments on composite sandwich plates. J. Shock Vib. 2014;15:184–8.
[5] Liu G, Li XD, Zhang Y. Numerical simulation of combined damage of fragments and shock wave on helicopter rotor. Comput. Simul. 2013;6:19.
[6] Hou H, Zhang C, Li M, Hu N, Zhu X. Damage characteristics of sandwich bulkhead under the impact of shock and high-velocity fragments. Explos Shock Waves 2015;1:116–23.
[7] Leppänen J. Dynamic behaviour of concrete structures subjected to blast, fragment impacts, Licentiate thesis, Department of Structural Engineering. Göteborg, Sweden: Concrete Structures,Chalmers University of Technology; 2002. p. 71.
[8] Leppänen J. Experiments and numerical analyses of blast and fragment impacts on concrete. Int J Impact Eng 2005;31(7):843–60.
[9] Schleyer Graham K, Underwood Nicholas J, Do Hyung Min, et al. On pulse pressure loading of plates with holes[J]. Cent Eur J Eng 2012;2(4):496–508.
[10] Rakvåg KG, Underwood NJ, Schleyer GK, et al. Transient pressure loading of clamped metallic plates with pre-formed holes [J]. Int J Impact Eng 2013;53:44–55.
[11] Hou J, Jiang J, Men J, et al. Dynamic response of thin plate with holes under blast loading [J]. Explos Shock Waves 2013;33(6):662–6 [in Chinese)].
[12] Jiang J, Hou J, Men J, et al. Study on deformation of perforated plates under blast loading [J]. Chin. J. High Pressure Phys. 2014;28(6):723–8 [in Chinese)].
[13] Li Ying, Wu Weiguo, Zhu Haiqing, et al. The in fluence of different pre-formed holes on the dynamic response of square plates under air-blast loading [J]. Eng Fail Anal 2017;78:122–33.
[14] Wu Jianyuan, Chong Ji, Yuan Long, et al. Dynamic responses and damage of cylindrical shells under the combined effects of fragments and shock waves[J]. Thin-Walled Struct 2017;113:94–103.
[15] Aune V, Valsamos G, Casadei F, et al. On the dynamic response of blast-loaded steel plates with and without pre-formed holes[J]. Int J Impact Eng 2017;108:27–46.
[16] LSTC. LS-DYNA Version 971 keyword User's Manual_Rev5-beta. Livermore Software Technology Corporation; 2010. p. 49–51.
[17] Jing L, Wang Z, Zhao L. Dynamic response of cylindrical sandwich shells with

metallic foam cores under blast loading – numerical simulations. Compos Struct 2013;99:213–23.
[18] Jing L, Xi C, Wang Z, Zhao L. Energy absorption and failure mechanism of metallic cylindrical sandwich shells under impact loading. Mater 2013;52:470–80.
[19] Li W, Huang GY, Bai Y, et al. Dynamic response of spherical sandwich shells with metallic foam core under external air blast loading–Numerical simulation [J]. Compos Struct 2014;116:612–25.
[20] Jing L, Yang F, Wang Z, Zhao L. A numerical simulation of metallic cylindrical sandwich shells. Latin Am J Solids Struct 2013;10:631–45.
[21] Hallquist JO. Ls-Dyna theory manual. Livermore Software Technology Corporation; 2006.
[22] Johnson GR, Cook WH. A constitutive model and data for metals subjected to large strains, high strain rates and high temperature [C]Proceedings o f the Seventh International Symposium on Ballistics, Netherlands. 1983.
[23] Glenn RP, Kenneth AB. Airblast loading model for DYNA2D and DYNA3D. ARL report; 1997.
[24] Bai Y, Wierzbicki T. A new model of metal plasticity and fracture with pressure and Lode dependence. Int J Plasticity 2008;24(749 – 6419):1071–96.
[25] Bao Y, Wierzbicki T. On fracture locus in the equivalent strain and stress triaxiality space. Int J Mech Sci 2004;46(1):81–98.
[26] Abushawashi Y, Xiao X, Astakhov V. A novel approach for determining material constitutive parameters for a wide range of triaxiality under plane strain loading conditions. Int J Mech Sci 2013;74:133–42.
[27] Bai Y, Teng X, Wierzbicki T. On the application of stress triaxiality formula for plane strain fracture testing. ASME J Eng Mater Technol 2009;131(2):021002.
[28] Wang B, Xiao XR, Astakhov Viktor P, Liu ZQ. The effects of stress triaxiality and strain rate on the fracture strain of Ti6Al4V[J]. Eng Fract Mech 2019;(219):106627.

Please cite this article as: Li W et al., The deformation and failure mechanism of cylindrical shell and square plate with pre-formed holes under blast loading, Defence Technology, https://doi.org/10.1016/j.dt.2020.06.014